Available online at www.sciencedirect.com
ScienceDirect
Journal of Nuclear Materials 375 (2008) 95–101
journal of nuclear materials
www.elsevier.com/locate/jnucmat

Influence of Portevin–Le Chatelier effect on rupture mode of alloy 718 specimens

V. Garat [a,*], J.-M. Cloue [a], D. Poquillon [b], E. Andrieu [b]

[a] AREVA, AREVA NP, Fuel Business Unit 10, rue Julietter Récamier, 69456 Lyon cedex, France
[b] CIRIMAT, UMR CNRS 5085, 118, route de Narbonne, 31077 Toulouse cedex 04, France

Received 4 April 2007; accepted 26 October 2007

Abstract

A set of tensile tests has been carried out under air environment in the temperature range (450–700 °C) in order to characterize the interactions between oxidation assisted intergranular cracking and Portevin–Le Chatelier effect. It is shown that the occurrence of jerky flow stops the intergranular damaging mechanism. The construction of a temperature versus strain rate diagram showing dynamic strain aging, intergranular fracture and PLC instabilities locations is then proposed. The surprising relation between crack initiation disappearance and PLC instabilities of type C in the temperature range explored is discussed. Finally the assumption of the occurrence of such phenomenon at the tip of a propagating crack is addressed.

PACS: 81.05.Bx; 81.40.Lm; 81.70.Bt

1. Introduction

Jerky flow, also known as Portevin–Le Chatelier effect, was first observed in Al–Cu alloys [1] and, afterwards, has been studied intensively in other dilute metallic alloys especially in steels, aluminium and nickel based alloys [2–5]. Physical processes involved in this type of flow instability as well as the associated localization of the deformation have been modelled and simulated [6–8]. Recent improvements of measuring techniques for deformation fields [9] offer the possibility to check those simulations under several aspects (localization, spatial coupling between bands, bands width). Nevertheless, a few studies are dealing with the role of grain boundaries on PLC plastic instabilities [10–12] and consequently, there is a lack of knowledge on the effect of this phenomenon on the evolution of intergranular internal stresses. An interesting way to study this particular point can be found in the scientific field dealing with oxidation assisted intergranular cracking (OAIC) because, in most of the cases, this damaging process requires to operate an intergranular oxidation process together with a high level of intergranular internal stresses. Fournier et al. [13] have clearly shown that the occurrence of PLC instabilities in alloy 718 during slow strain rate tests at 400 °C stops immediately the intergranular crack propagation.

The aims of the present paper are firstly, to bring new experimental results completing at higher temperature the work undertaken by Fournier et al. and then, to evaluate the interactions between crack initiation and localization of plastic instabilities. As strain rate controlled tensile tests have been carried out on a thin strip, both crack initiation and propagation sensitivity to dynamic strain aging (DSA) have been investigated.

2. Materials and experimental procedure

The material used in this study was obtained through a double melting process: vacuum induction melting plus vacuum arc remelting. The nominal composition of the alloy is given in Table 1. The cast ingot was hot and cold

* Corresponding author. Tel.: +33 4 72 74 82 03; fax: +33 4 72 74 88 33.
E-mail address: veronique.garat@areva.com (V. Garat).

0022-3115/$ - see front matter © 2007 Elsevier B.V. All rights reserved.
doi:10.1016/j.jnucmat.2007.10.009

Table 1
Chemical composition of the alloy 718 strip (wt%)

Ni	Cr	Mo	Fe	Ti	Al	Nb + Ta
bal	18.1	2.88	18.3	1.04	0.54	5.15

rolled down to a thickness of 1 mm, followed by a solution annealing heat treatment at 1000 °C for 1 h ended by air quenching.

Tensile specimens (dimensions are given in Fig. 1) were then electro-discharge machined and heat treated under vacuum following the usual heat treatment: 720 °C/8 h then cooling 50 °C/h down to 620 °C with a 8 h hold time. The material is fully recrystallized and free of delta phase, as can be observed in Fig. 2. Finally, samples were thinned by mechanical grinding down to 0.3 mm all along the gauge length and mechanically polished by using SiC paper and diamond paste down to the grade 1 μm. This thinning process aimed at increasing the damaging effects of environment through a reduction of the ratio volume/surface.

Mechanical tests were performed with two different types of machines. The first one is a hard electro-mechanical tensile machine with displacement rate control. The

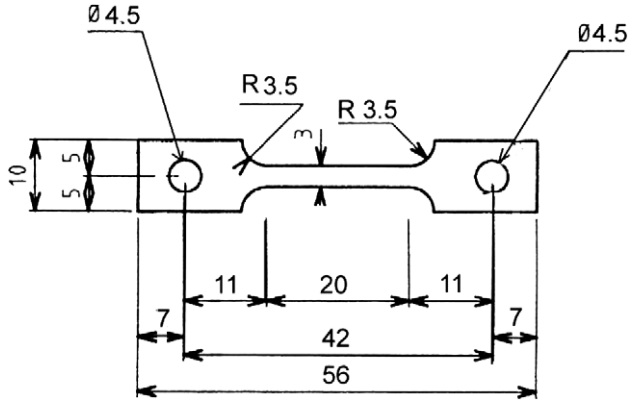

Fig. 1. Tensile thin specimen (thickness = 0.3 mm).

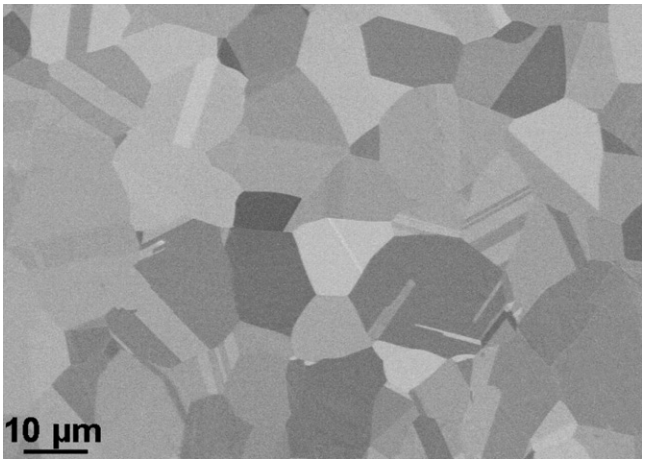

Fig. 2. Microstructure of thin strip material, after etching – SEM, backscattered beam.

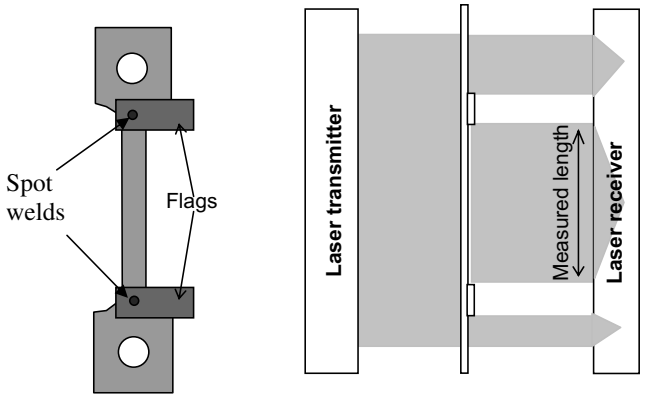

Fig. 3. Laser device for specimen elongation measurement. Front and side views.

second one is a soft creep machine which was adapted in order to control the loading rate: the loading was imposed by a constant and controlled water flow flowing into a basket hanged on the loading arm of the creep machine. This was done in order to prevent any specimen discharge during the tensile test when serrations would occur. Indeed, standard computer-driven machines are not fast enough to counteract the serrations.

In both cases, a laser extensometer was used to measure the deformation of the specimens (see Fig. 3). Heating was ensured by a three zones radiation furnace which allows controlling precisely (±1 °C) specimen temperature all along the gauge length in the considered temperature range (20–700 °C). Tests were performed under laboratory air and, when necessary, the oxygen partial pressure was decreased by means of a vacuum device and/or hydrogenated argon (5% H_2). Fractured samples were observed by SEM (LEO 435 VP).

3. Experimental results

3.1. Effect of environment

In order to evaluate the specific role of oxidation on the occurrence of intergranular fracture in the dynamic strain aging domain, several tensile tests were performed at 650 °C/10^{-3} s^{-1} either under laboratory air or under hydrogenated argon. As expected, the fracture surface was fully transgranular ductile under hydrogenated argon while intergranular brittle fracture areas as well as intergranular cracks all along the gauge length were observed on specimens tested under air environment (see Figs. 4 and 5). The global mechanical response of these flat and smooth specimens indicates that the material of the study is sensitive both to oxidation assisted crack initiation and to intergranular crack propagation.

3.2. Characterization of PLC types

As an example, Fig. 6 shows the type of serration on the stress–strain curve recorded when PLC occurred in the

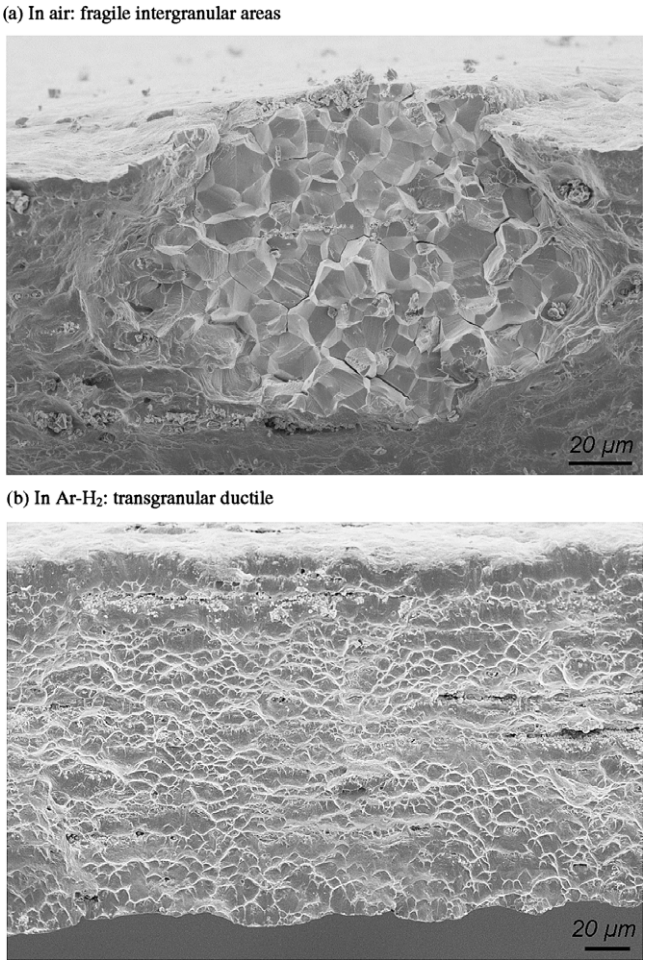

Fig. 4. Rupture paths – SEM.

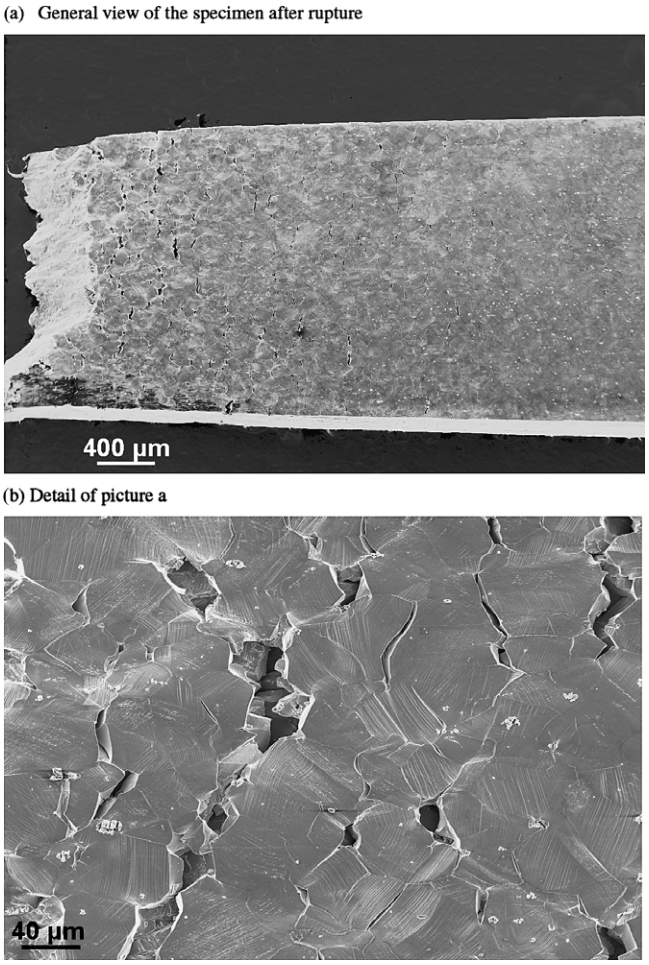

Fig. 5. Gage of a specimen showing intergranular rupture – SEM.

explored temperature–strain rate domain. The amplitude of the serrations is rather regular and lead to a stress drop close to 75 MPa below the average level of the curve; each serration is linked to the emission of an audible characteristic noise. Fig. 6 also presents strain and stress versus time, in the serrations domain. According to Klose et al. [14], those serrations are either of type B or type C. Rodriguez [15] defines type C PLC when serrations produce load drop below the general level of the stress–strain curve. They appear at high temperature and low strain rate, the critical deformation for the onset of PLC increases when temperature increases (or strain rate decreases). Fig. 7 shows that, in the temperature range of this study, the critical strain for the onset of serrations for the thin strip of alloy 718 increases with increasing temperature. We can conclude that, in these testing conditions, the serration type observed on the alloy 718 is type C. This type is associated with the random nucleation of deformation bands all along the specimen length.

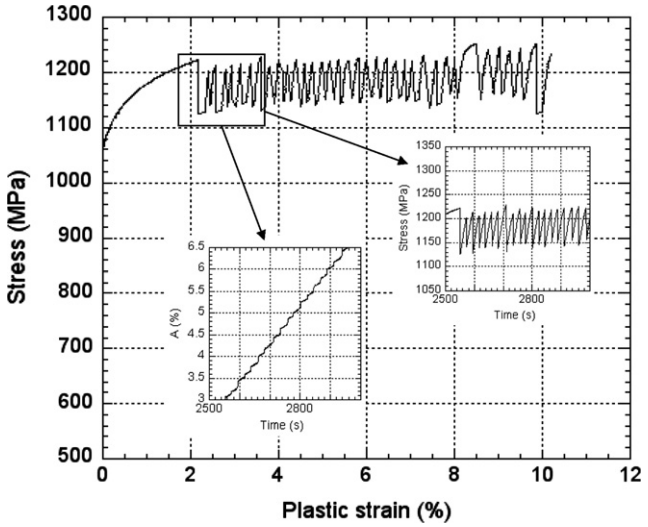

Fig. 6. Stress–strain curve at 570 °C and 10^{-3} s^{-1} (laboratory air).

3.3. Experimental construction of a DSA-fracture mode-PLC map

In the temperature range (450–700 °C), various tensile tests were carried out under air testing conditions at different strain rates. The results obtained both in terms of flow mode and fracture mode are presented in Fig. 8. As a complement, the results obtained previously by Fournier et al. [13] at low strain rate (5×10^{-7} s^{-1}) are recalled on this

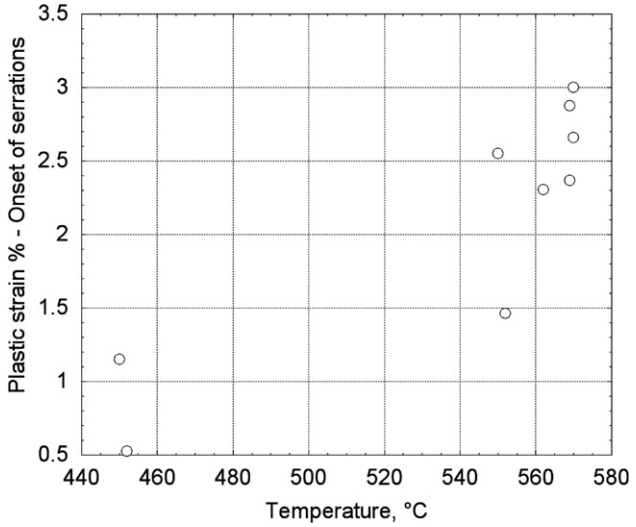

Fig. 7. Evolution of the onset of serrations (critical plastic strain) as a function of temperature.

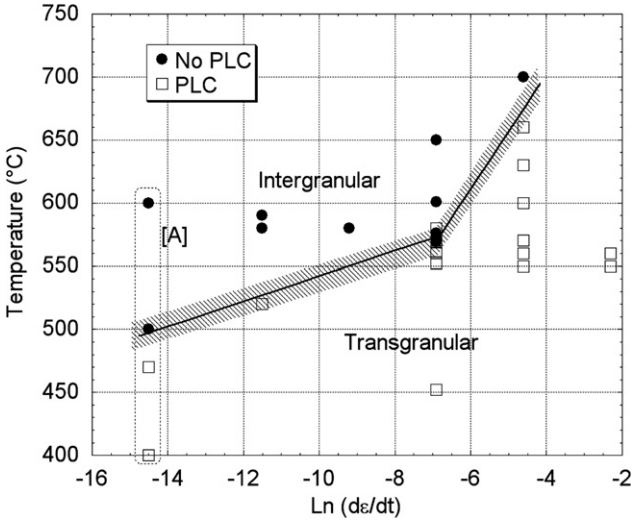

Fig. 8. Rupture modes and plastic flow modes map. Points in the dash box [A]: data from Fournier [13].

plot. Rupture paths observed by SEM show systematically that above 450 °C the fracture is transgranular ductile when PLC triggers on whereas an intergranular brittle mode of fracture is observed in the other cases. This experimental fact is so systematic that a single border can be drawn which separates both smooth from serrated plastic flow and intergranular fracture from transgranular ductile.

It is worth mentioning here that when the testing mechanical conditions are located in the left part of the map, any thermo-mechanical modification that initiates PLC instabilities will stop the intergranular damaging process. Temperature drop (25 °C) or two unloading cycles with an amplitude of 200 MPa at 600 °C can initiate PLC instabilities and stop OAIC. Moreover, for the same testing conditions in the vicinity of the PLC border, a specimen can exhibit serrations while another may not. The PLC border is indeed a thick line of about ±20 °C around the line indicated in Fig. 8 within which serration can occur or not. In any case, it's worth noticing that the PLC occurrence always corresponds to a fully transgranular ductile rupture mode while, when serrations do not occur, fragile intergranular areas are observed on the rupture path.

4. Discussion

This interaction between PLC serrations and rupture mode raises various questions as it could be due to very different root phenomena. Indeed, OAIC implies a compatibility between oxidation kinetics and both initiation and propagation rates. OAIC needs also a loading which raises the grain boundary stress above their opening threshold. On the other hand, PLC serrations lead to specimen unloadings, they modify the deformation paths and kinetics and they interact with some of the material solutes. In a first part, we will try to identify which phenomenon is involved in this systematic interaction between PLC and fracture mode. In a second part, we will focus on what happens at the crack tip when PLC is activated. Is there a relation between this phenomena and the crack growth rate limitation at high temperature?

4.1. On the understanding of the interactions between PLC and rupture mode

4.1.1. Kinetics effects

In order to stabilise temperature and oxidation conditions, each specimen is held at the testing temperature during 10 min before the test starts.

Several specimens were tested in the same conditions and, in the temperature and strain rate around the PLC/no PLC border (see Fig. 8, 570 °C – 10^{-3} s^{-1}), some specimens showed serrated yielding and others did not. Each time, the correlation has been confirmed between PLC occurrence and transgranular ductile rupture. As temperature is the same during these tests, oxidation kinetic is similar for these specimens while fracture modes are different.

Thus, the assumption according to which, in this temperature range and above, the oxidation rate is fast enough to be considered as a non-limiting parameter in the global damaging process seems to be valid. However, the validity of this assumption has to be reconsidered when dealing with a lower temperature range.

4.1.2. Mechanical unloading during serrations

A large number of studies have been devoted to the effect of unloading or overloading on fatigue crack growth. Creep–fatigue crack growth rate in alloy 718 and more particularly in N18 alloy is known to be markedly reduced when an unloading of at least 5% is applied at the beginning of the hold time period [16,17]. This unloading sequence generates a compression zone at the crack tip which stops or delays the OAIC damaging process. Thus, assuming that a crack initiates when the local propagation

conditions are met, i.e. when at least the crack tip does not undergo compression, a possible effect of repeated macroscopic unloadings on the crack initiation has to be considered. In order to try to clarify this point, two different tests were performed under air environment.

- During a constant strain rate test (10^{-3} s^{-1}) at 650 °C, unloading–loading cycles with an amplitude equal to 200 MPa were superimposed. With these testing conditions, PLC instabilities do not initiate and finally the fracture surface exhibits intergranular fracture areas.
- At 560 °C, some tests were performed on the smooth constant loading machine, with a constant stress rate of 1.5 MPa s^{-1}. At this strain rate, plastic deformation bands propagate during the test. The fracture surface is fully ductile even if, thanks to the loading system, the macroscopic loading rate is kept $\geqslant 0$. Due to the fact that these testing conditions were chosen close to the PLC threshold at this temperature, it was possible to have in the same testing conditions a mechanical response without instability. In this latter case, the fracture surface exhibits intergranular fracture areas.

From these complementary tests it seems that serrations, seen as repeated sequences of macroscopic unloading of the specimen, are not responsible for the disappearance of the intergranular fracture mode.

4.1.3. Relation between PLC serrations and rupture mode

More than 50 specimens have been tested in this temperature range and the result is always the same: there is a correlation between crack initiation and PLC initiation. The randomness of these two phenomena is often assumed. The results presented in this study suggest that these phenomena are linked in terms of initiation site.

When intergranular crack initiation is possible, SEM observations all along the gauge length show that the location of the intergranular crack initiation sites is not related to primary carbide alignments but randomly distributed on the whole specimen surface.

Various authors intended to understand and to visualise PLC bands propagation, as in aluminium alloys by using a laser scanning extensometer [14,18] or by using finite element methods and applying a jerky flow law on a polycrystal model [19]. These studies show that when type C instabilities occur it seems that randomly distributed local strain jumps are observed.

The alloy 718 is known to localize considerably the deformation into bands, around the grain boundaries and, if any, at the defect tips. As PLC start needs to have reached a critical plastic strain, we can assume that such an erratic type C PLC will begin first in these high-strained and high-stressed regions.

OAIC occurs when there is compatibility between oxidation kinetic and initiating (and later propagating) rate. If PLC suppresses OAIC, it may be because it disturbs one or both aspects: decrease of the local stress level and/or slowing down the embrittlement process. Indeed, on the one hand, several studies have shown that oxygen diffuses in grains boundaries [20] and reduces the cohesion stress of the grain boundaries. On the other hand, these local strain jumps could allow releasing internal intergranular stresses, which may prevent crack initiation.

4.1.4. Are there any interactions between PLC bands and a crack tip?

The use of the present results to explain changes of fracture mode in high temperature creep–fatigue is addressed in this part of the paper. The problem can be stated as follows: Assuming that it is possible to trigger PLC instabilities in the plastic zone of a propagating crack under small scale yielding conditions, does the maximum intergranular creep crack growth rate associated with a given microstructure can be related to the maximum local strain rate and cumulative deformation that the material can sustain before triggering PLC instabilities? Applicability of this idea to the crack front of a real crack in a polycrystalline material implies that as stress intensity factor increases, the number of grains included in the plastic zone ahead of the crack front that meet the criteria for PLC triggering increases too.

Indeed, high temperature crack propagation resistance of alloy 718 depends on several materials variables (grain size, heat treatments, deformation mechanisms, delta phase precipitation) but under air testing conditions, intergranular cracking is often reported and linked to specific local loading conditions together with oxidation processes. In order to get experimental data on a microstructure representative of the one used in the present study, results published by Pedron and Pineau [21] were used. From these studies the maximum creep–fatigue intergranular cracking rate was estimated equal to 1.7 μm/s by assuming that crack propagates essentially during the hold time i.e. during the creep stage of the loading cycle.

What happens at a crack tip when the propagating conditions are close to the PLC threshold? Is there a link between the crack propagation transition observed in fatigue tests and the occurrence of serrated yielding? Indeed, at the crack tip, the mechanical loading is localized (small scale yielding). We must consider a statistical average of grains boundaries loading. Moreover, the size of the loaded area is relatively small in alloy 718 and increases as the crack propagates. How can we make a link between the smooth polycrystal specimens tested here (20 μm grain size) and the crack tip region? A finite element analysis was performed using CAST3M finite element code [22], modelling a compact tensile (CT) specimen in alloy 718 with a crack, loaded by a constant opening. A 2D plane stress analysis is carried out. The crack length is short enough (see Table 2) so that the strain path does not vary much during the crack propagation. The main characteristics of the modelling are detailed in Table 2.

Fig. 9 shows how the strain rate was calculated for two different crack lengths. A first strain field, corresponding to

Table 2
Characteristics of CAST3M modelling

Crack length, a (m)	1.26E−2
a/W of CT specimen	0.315
K_I (MPa m$^{1/2}$)	28.5
Temperature (°C)	650
Material behaviour	Elastic–plastic
Young Modulus (GPa)	160
Yield strength (MPa)	1000

an initial crack length ($a = 12.6$ mm) is computed. Then the mechanical state is computed for the same loading (corresponding to $K_i = 28.5$ MPa m$^{1/2}$) but with an increment $da = 10$ μm of the crack length. So, two distinct elasto-plastic calculations for two close values of the crack length are carried out under monotonic loading. Then, a strain rate at any point in the plastic zone is obtained by differentiating between these two strain states. In Fig. 10, plastic strain rate is plotted as a function of the distance to the initial crack tip for two crack propagation rates: 0.2 μm/s and 5 μm/s. The first one is one order of magnitude below the transition rate [17–21], the second one is above. On this plot are also represented the local 3% strain limit (dash points) and the strain rate PLC threshold deduced from Fig. 8 (plane curve). As expected, the fastest the macroscopic crack propagation rate, the largest the local strain rate around the crack tip. For a propagation rate of 0.2 μm/s, the whole crack tip exhibits a slower strain rate that the threshold rate for the occurrence of serrated yielding. On the contrary, for a 5 μm/s crack propagation rate, a 60 μm wide zone at the crack tip experiences mechanical conditions which should lead to PLC. For intermediate propagating rates, the size of the zone where local strain rate is high enough to promote PLC reduces as the crack propagation rate decreases. The elasto-plastic behaviour of alloy 718, which exhibits very little hardening, is responsible for the localisation of the plastic strain at the crack tip.

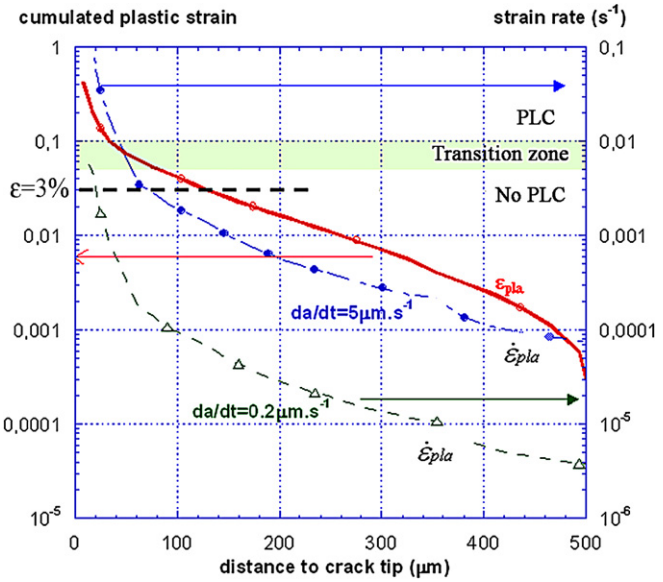

Fig. 10. Plastic strain and plastic strain rate values in front of the crack tip of a CT specimen ($a/W = 12.6$ mm/40 mm $= 0.315$; $K_I = 28.5$ MPa m$^{1/2}$) calculated by finite element modelling (see Fig. 9) for two crack propagation rates (0.2 and 5 μm s^{-1}). The solid line represents the equivalent cumulated plastic strain (left y-axis). The dashed lines represent the strain rate for the two different propagation rates (right y-axis).

It has to be pointed out that as finite element calculations have been carried out without implementing any crack propagation, such an approach tends to overestimate the strain rate in the plastic zone for power-law hardening material. This point has been studied by Rice and Sorensen [23]. They have shown that deriving crack-tip analytical strain field (HRR) predicted by Hutchinson–Rice–Rosengren [24,25] at the tip of a moving crack leads to a singular distribution of the strain rate. They have also used finite element calculations available in 1978 to prove that the singularity in plastic zone of a moving crack was overestimated when calculations were performed by translating HRR singularity. So, in the present work, the material

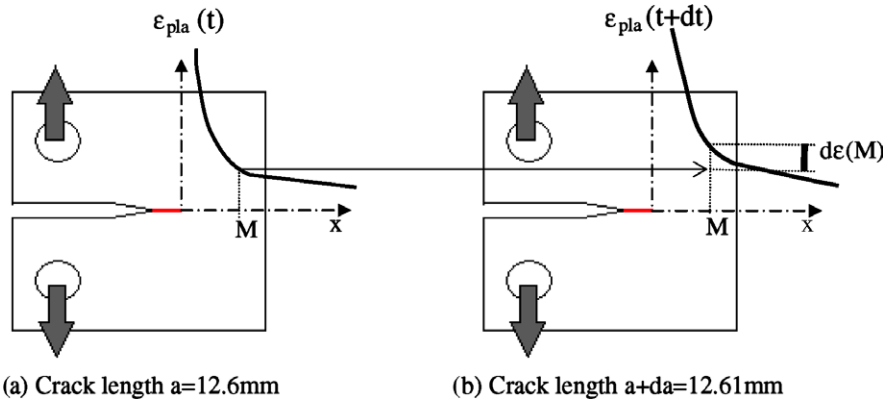

Fig. 9. Scheme of the finite element elasto-plastic computations (using CAST3M) carried out in this study in order to get the equivalent plastic strain at the crack tip. (a) Initial state, crack length $a = 12.6$ mm ($W = 40$ mm; $a/W = 0.315$; $K_I = 28.5$ MPa m$^{1/2}$); (b) after a small crack advance of $da = 10$ μm, $a = 12.61$ mm; x stands for the distance to the initial crack tip, point M equivalent plastic strain increases by $d\varepsilon$, at a strain rate $d\varepsilon/dt$ and for a crack propagation rate da/dt.

exhibits very little hardening and do not follow a power-law hardening behaviour. However, strain rates are calculated by translating two strain states. This method does not take into account the fact that a moving crack contained a zone of elastic unloading in the wake of the crack and may also overestimate the strain rate at the crack tip. But as in the present study, analysis is carried out in terms of orders of magnitude, this approach is sufficient. However, a node-release finite element simulation would give more accurate results.

Finally, the PLC transition rate observed in this study is of the same order of magnitude as the transition rate for propagation mode observed by Pedron [21] during creep–fatigue tests. Indeed the scale of the loading has to be compared to the grain size so that it is understood that instabilities can develop in parts of the grains. This point is consistent with the fact that in this alloy, deformation is quite heterogeneously distributed in the grains and that PLC instabilities have been identified as type C. PLC deformation bands can on the one hand, redistribute the local stresses and on the other hand, they can also reduce the flux of embrittling species to the grain boundaries.

5. Conclusions

The present investigation into the interactions between oxidation assisted intergranular cracking, dynamic strain aging and PLC instabilities has shown that in a rather large temperature range, the occurrence of PLC instabilities inhibits OAIC. The PLC bands have been identified as type C bands. As there is a striking relation between serration occurrence and the disappearance of intergranular crack initiation sites, it is proposed that the nucleation sites of strain jumps are located in the same areas in the polycrystal. The question of the applicability of this phenomenon at the tip of a propagating crack to explain the upper limit of the creep crack growth rate has been addressed. The local strain rate corresponding to the change of crack propagation mode from intergranular to transgranular is of the same order of magnitude as the applied strain rate which PLC instabilities appear in uniaxial tension at 650 °C.

Acknowledgements

The authors are grateful to several students from ENSI-ACET namely S. Robert, B. Meunier, M. Campo and L. Crayssac who have performed most of the tensile tests and SEM observations and would like to thank AREVA-NP Company for its financial support.

References

[1] A. Portevin, F. Le Chatelier, Compte rendu de l'Académie des Sciences, Paris 176 (1923) 507.
[2] R.A. Mulford, U.F. Kocks, Acta Metall. 27 (1979) 1125.
[3] L.P. Kubin, Y. Estrin, J. Phys. III (1991) 929.
[4] C.L. Hale et al., Mater. Sci. Eng. A 300 (2001) 153.
[5] J.P. Balik et al., Scripta Mater. 42 (2000) 465.
[6] A.H. Cottrell, Dislocations and Plastic Flow in Crystals, Oxford University, London, 1953.
[7] J. Friedel, Dislocations, Pergamon, Oxford, 1964.
[8] L.P. Kubin et al., in: F.R.N. Nabarro, M.S. Duesberry (Eds.), Dislocations in Solids, vol. 11, Elsevier, Amsterdam, 2002, p. 101.
[9] H. Neuhäuser et al., J. Alloys Comp. 378 (2004) 13.
[10] H.M. Zbib, E.C. Aifantis, Res. Mech. 23 (1988) 261.
[11] A. Kalk et al., Philos. Mag. A 72 (1995) 1239.
[12] Zs. Kovacs et al., J. Eng. Mater. Technol. 124 (2002) 23.
[13] L. Fournier et al., Mater. Sci. Eng. A 316 (2001) 166.
[14] F.B. Klose et al., Comput. Mater. Sci. 26 (2003) 80.
[15] P. Rodriguez, S. Venkadesan, Key Eng. Mater. 103 (1995) 257.
[16] E. Andrieu, A. Pineau, J. Phys. IV 9 (9) (1999) 3.
[17] A. Pineau, in: R.P. Gangloff, M.B. lves (Eds.), Proceedings of the International Conference on Environment-induced Cracking of Metals (Nace-10, 2–7 October 1998), 1990, p. 111.
[18] A. Ziegenbein et al., Comput. Mater. Sci. 19 (2000) 27.
[19] S. Kok et al., Acta Mater. 51 (2003) 3651.
[20] S. Perusin, D. Monceau, E. Andrieu, J. Electrochem. Soc. 152 (12) (2005) E390.
[21] J.P. Pedron, A. Pineau, Mater. Sci. Eng. 56 (2) (1982) 143.
[22] CAST3M <http://www-cast3m.cea.fr/cast3m/index.jsp>.
[23] B. Rice, E.P. Sorensen, J. Mech. Phys. Solids 26 (3) (1978) 163.
[24] J.W. Hutchinson, J. Mech. Phys. Solids 16 (1968) 337.
[25] J.R. Rice, G.F. Rosengren, J. Mech. Phys. Solids 16 (1968) 1.